Ann. Geophys., 24, 555–566, 2006
www.ann-geophys.net/24/555/2006/

Annales Geophysicae

Thermospheric gravity waves in Fabry-Perot Interferometer measurements of the 630.0 nm OI line

E. A. K. Ford, A. L. Aruliah, E. M. Griffin , and I. McWhirter

Atmospheric Physics Laboratory, Department of Physics and Astronomy, University College London, Gower Street, London, WC1E 6BT, UK

Received: 17 August 2005 – Revised: 24 November 2005 – Accepted: 16 January 2006 – Published: 23 March 2006

Abstract. Gravity waves are an important feature of mesosphere – lower thermosphere (MLT) dynamics, observed using many techniques and providing an important mechanism for energy transfer between atmospheric regions. It is known that some gravity waves may propagate through the mesopause and reach greater altitudes before eventually "breaking" and depositing energy. The generation, propagation, and breaking of upper thermospheric gravity waves have not been studied directly often. However, their ionospheric counterparts, travelling ionospheric disturbances (TIDs), have been extensively studied in, for example, radar data. At high latitudes, it is believed localised auroral activity may generate gravity waves in-situ. Increases in sensor efficiency of Fabry-Perot Interferometers (FPIs) located in northern Scandinavia have provided higher time resolution measurements of the auroral oval and polar cap atomic oxygen red line emission at 630.0 nm. A Lomb-Scargle analysis of this data has shown evidence of gravity wave activity with periods ranging from a few tens of minutes to several hours. Oscillations are seen in the intensity of the line as well as the temperatures and line of sight winds. Instruments are located in Sodankylä, Finland; Kiruna, Sweden; Skibotn, Norway, and Svalbard in the Arctic Ocean. A case study is presented here, where a wave of 1.8 h period has a phase speed of 250 ms^{-1} with a propagation angle of 302°, and a horizontal wavelength of 1600 km. All the FPIs are co-located with EISCAT radars, as well as being supplemented by a range of other instrumentation. This allows the waves found in the FPI data to be put in context with the ionosphere and atmosphere system. Consequently, the source region of the gravity waves can be determined.

Keywords. Ionosphere (Ionosphere-atmosphere interactions) – Meterology and athmospheric dynamics (Thermospheric dynamics; waves and tides)

Correspondence to: E. A. K. Ford
(elaina.ford@ucl.ac.uk)

1 Introduction

Atmospheric gravity waves are an important mechanism for the transfer of energy and momentum throughout the atmosphere. Gravity waves have mostly been studied in the stratosphere, mesosphere, and lower thermosphere regions as these have the largest powers and so have a significant role. At higher altitudes, AGWs are important as they can transport energy and momentum large distances, for example, redistributing energy to equatorial latitudes. However, most high-latitude studies have been on Travelling Ionospheric Disturbances (TIDs), the ionospheric reaction to AGWs (see for example Balthazor and Moffett, 1999; MacDougall et al.; 2001; Arnold et al., 1998, and reviews by Hunsucker, 1982; Williams et al., 1993; Hocke and Schlegel, 1996). Gravity waves have been observed in the upper thermosphere over the southern polar cap, for example, by de Deuge et al. (1994) and Innis et al. (2001) with photometer observations of the 630.0 nm oxygen emissions and by Innis and Conde (2002) in satellite data. Innis and Conde (2001) observed gravity waves in vertical thermospheric winds from the Dynamics Explorer 2 (DE2) satellite.

Gravity waves at lower altitudes mostly have their origin in the troposphere. They are formed from, for example, thunderstorms or air rising over mountain ranges. Amplitudes of the waves increase with decreasing density at increasing altitudes. The gravity waves that are formed in the troposphere have mostly dissipated long before they reach F-region altitudes. Gravity waves observed here therefore have to be created in situ in the thermosphere. The mechanisms to create these gravity waves are auroral in origin. Large-scale gravity waves are thought to be generated in magnetic storms by one of two mechanisms. Particle precipitation in auroral regions will create localised heating that could set off waves, as could the Lorentz forces and Joule heating from electrojet currents (de Deuge et al., 1994). The theory of gravity wave behaviour and the expected properties of the waves have been reviewed by Hunsucker (1982) and Hocke and Schlegel (1996).

Published by Copernicus GmbH on behalf of the European Geosciences Union.

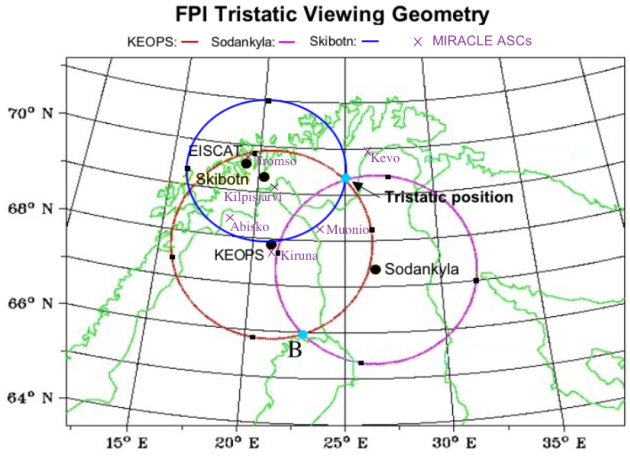

Fig. 1. Fields of view of the three FPIs at Skibotn, KEOPS and Sodankylä and the EISCAT radar at Tromsø, for elevation angles of 45° for KEOPS and Sodankylä and 51.5° for Skibotn. The dots indicate the positions of the volumes viewed by each FPI. Positions A and B are the tristatic and bistatic volumes, respectively, and there is a near tristatic position vertically above KEOPS. Locations of some of the IMAGE magnetometers are also given.

The aim of this paper is to show gravity waves have been found in the upper thermosphere in the northern auroral oval and polar cap regions, in neutral atom emission intensities as well as temperatures and winds. This is believed to be the first detection of gravity waves in upper thermospheric temperatures. The array of measurements obtained will allow phases of the wavefronts to be calculated so that the source region and therefore mechanism of the waves can be identified. A case study of the night of the 25 November 2003 is used, where EISCAT radar data is available viewing the same volume of atmosphere as the FPIs. Use is also made of the many other instruments available in the area.

2 Data and analysis

The University College London (UCL) Fabry-Perot Interferometers (FPIs) measure the atomic oxygen red line emission at 630.0 nm, which has a peak intensity at about 240 km altitude (Solomon et al., 1988). Temperatures and wind velocities of the neutral atmosphere are obtained as well as the intensity of the line emission. UCL has three FPIs, which are located in the auroral oval in Sodankylä, Finland (67.4° N, 26.6° E), KEOPS (Kiruna Esrange Optical Site), Sweden (67.8° N, 20.4° E), and in the polar cap at Longyearbyen on Svalbard (78.2° N, 15.6° E) (Aruliah and Griffin, 2001). Collaborations on a campaign basis with the University of Lancaster, which has an FPI in Skibotn in northern Norway (69.3° N, 20.4° E), allow us to take tristatic measurements with the three FPIs in northern Scandinavia. The geometry of this tristatic setup can be seen in Fig. 1. All these FPIs are co-located with EISCAT radars at Tromsø (Norway), Kiruna (Sweden), and Sodankylä (Finland) (e.g. Rishbeth and Williams, 1985). For the night of the data presented here, the EISCAT tristatic point was over the KEOPS zenith position, at an altitude of 240 km. A range of other instrumentation in the region also supplements the FPI data. The fields of view of the CUTLASS and STARE coherent scatter radars also cover this region. CUTLASS measures plasma velocities using HF radar. It receives echoes from E and F region ionospheric irregularities, perpendicular to the direction of transmission, while STARE using VHF measures the E region to calculate electric fields. The IMAGE magnetometer network consists of 29 magnetometers across Scandinavia, covering the same region as the FPI look directions (e.g. Viljanen and Häkkinen, 1997) and there are all sky cameras (ASCs) at several of these locations, as part of the MIRACLE network.

Recent increases in the detector efficiencies of the FPIs have provided higher time resolution measurements of the thermosphere. The KEOPS FBI has the most sensitive detector, allowing integration times of 20 s, while Sodankylä and Svalbard have 40 s and Skibotn has 60 s. The FPIs look at a 1° field of view at an elevation angle of 45°, which with an emission altitude of 240 km provides viewing volumes shown by dots on the circles in Fig. 1. Data is taken in cycles, each looking at north, east, south, west, the tristatic A and bistatic B positions, the zenith and a calibration lamp. This leads to cycle times of 3.5 min for KEOPS, 8.5 min for Sodankylä, 13.9 min for Skibotn and 10.1 min for Svalbard (Skibotn takes longer due to a more complicated and slower mirror control system).

These cycle times in principle allow waves to be detected in the data of as short as 7-min periods for KEOPS or 17 and 28 min for Sodankylä and Skibotn respectively, i.e twice the period of observations. This gives a maximum detectable frequency (the Nyquist frequency) of 8.6 cycles per hour, for KEOPS data. For Svalbard, we also undertook a high-resolution vertical study, where just zenith measurements were taken, with a calibration exposure about every 12 min. This provided data about every minute; so all waves should be detectable down to the Brunt-Väisälä period, which at this altitude (240 km) is around 12 min (e.g. Hargreaves, 1979; Innis et al., 2001). Temporal resolutions as good as this are desirable for all data sets, so as to have sufficient sampling to be able to determine all waves down to 12 min. The longest periods detectable are up to half the period of darkness, which in the polar winter night extends up to 24 h per day for over three months. In practice though, only periods less than 6 h are included, as periods longer than this are hard to distinguish from atmospheric tides.

The time series analysis performed on these data was a Lomb-Scargle least squares frequency analysis of unevenly sampled data as first formulated by Lomb (1976) and further developed by Scargle (1982). This method was used to cope with the uneven sampling of the data. This can be due to

the inconsistencies in timing, over the many look directions observed in a cycle, created due to the scanning mechanism. In addition, the absence of data points, due to either cloud cover or the non-fitting of spectra due to low intensities will increase the unevenness of the sampling.

The amplitudes, $A(\omega)$, of the waves were calculated using Eq. (1) below from Hocke, (1998) for n data points, using the spectral power ($P_N(\omega)$) and the variance (σ^2) of the data.

$$A(\omega) = \sqrt{\frac{2}{n} 2\sigma^2 P_N(\omega)} \quad (1)$$

An IDL routine (Wilms, 2000; http://astro.uni-tuebingen.de/software/idl/aitlib/timing/-scargle.html) was used to analyse data, which calculates the spectral power of the normalised periodogram as a function of angular frequency, ω. It is normalised using the variance of the data as determined by Horne and Baliunas (1986), and it uses the fast algorithm described by Press and Rybicki (1989).

A cross correlation analysis of this temperature data can be used to obtain information on the wave speed, direction, and wavelength. A cross correlation between the north and south directions and the east and west directions will give, respectively, the meridional and zonal time lags τ_y and τ_x across the field of view of the FPI (e.g. Oliver et al., 1995). These lags will be dependant on the distance between the look directions (d), the phase speed of the wave (v) and the phase angle (θ, measured clockwise from north). These parameters can therefore be calculated with the following equations (Oliver et al., 1995):

$$v = \sqrt{\frac{d^2}{\tau_x^2 + \tau_y^2}} \qquad \theta = \arctan\frac{\tau_x}{\tau_y} \quad (2)$$

The distance, d, between the FPI look directions, presuming a fixed emission altitude of 240 km over the viewing area and with an elevation angle of 45°, is approximately 480 km. The horizontal speed of the wave can then be used, along with the frequency information from the Lomb-Scargle periodogram, to calculate the horizontal wavelength, λ_h, using $v{=}\omega/k$.

3 Results and discussion

3.1 Thermospheric data

The second UCL tristatic campaign, where the UHF EISCAT radars viewed the same common volume as the three FPIs, was on the night of the 25 November 2003. The first campaign, on the 27 February to the 1 March 2003 is discussed in Aruliah et al. (2004, 2005). The EISCAT data from the second campaign, on the night of the 25 November 2003, are shown in Fig. 2. It is a potentially good night to find gravity waves because TIDs appear to be present as clear wavefronts can be seen in the electron density (Fig. 2a). For example, a wavefront between 21:50 UT and 22:30 UT is highlighted with a dotted line. The wavefronts can also be seen, though

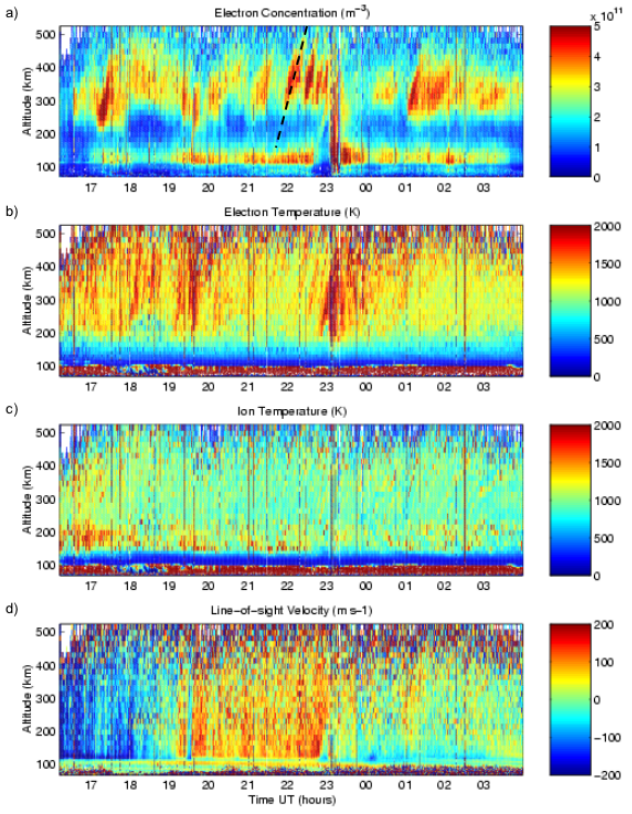

Fig. 2. EISCAT data from 25 November 2003, showing **(a)** electron density, **(b)** electron temperature, **(c)** ion temperature, and **(d)** ion velocity. A wavefront of a gravity wave in electron density is shown with a dashed line.

not as clearly, in the electron temperature data in Fig. 2b. The effect is even weaker in the ion temperatures of Fig. 2c. Figure 2d shows the line of sight velocities along the Tromsø beam (which at this time was towards the tristatic point over the KEOPS site). These do not show the wave structures due to the overwhelming effect of the diurnal change in direction due to the two-cell convection pattern of the polar cap region. These data are discussed further in Sect. 3.3, and observations of TIDs in EISCAT data are discussed in e.g. Williams et al. (1993), Lanchester et al. (1993), Shibata and Schlegel (1993), Mitchell and Howells (1998).

Figure 3 shows the 630.0 nm intensities from the tristatic campaign on the 25 November 2003. The look directions shown are towards the tristatic point above KEOPS, which is to the south of Skibotn and west of Sodankylä. A good correlation is seen between the sites, which shows that they are looking at a common volume of atmosphere. The slight discrepancies at 15:00–16:00 UT and 17:00–19:00 UT are most likely caused by the different instruments no longer looking at a common volume. This is often due to cloud cover which results in a loss of directional information due to scattering, and a decrease in signal to noise ratio. However, no clouds

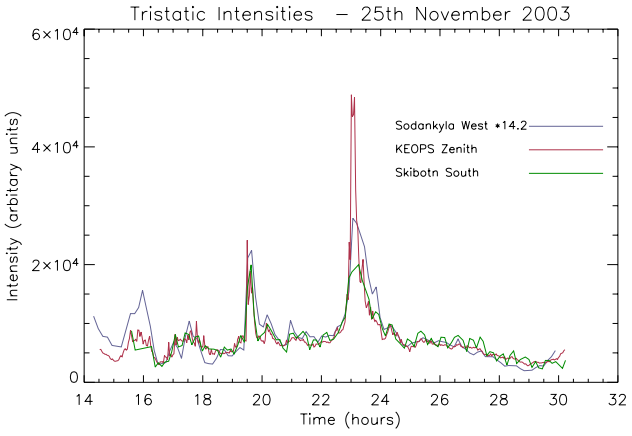

Fig. 3. 630.0 nm intensities from KEOPS, Sodankylä, and Skibotn on the 25 November 2003. As the intensities are not calibrated, the Sodankylä data are scaled to match the other sites by a factor of the ratios of the median value of Skibotn to Sodankylä data for this night. The directions shown point to the tristatic point above KEOPS.

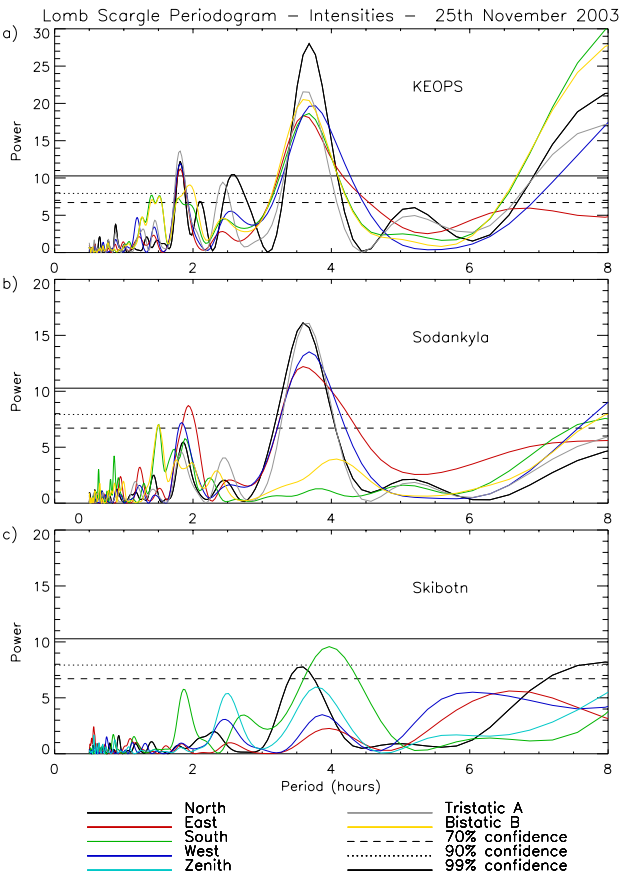

Fig. 4. Lomb-Scargle periodograms for **(a)** KEOPS **(b)** Sodankylä and **(c)** Skibotn FPI intensities on the 25 November 2003. Colours represent the different look directions observed, and horizontal lines are 70%, 90% and 99% confidence levels.

were observed that night, and all sky cameras and satellite images show clear skies. The other reason for the intensities not matching is due to the height of the atomic oxygen layer changing. This will result in the viewing volumes over- or under-shooting the tristatic volume so that they are no longer all viewing a common volume. This is covered thoroughly by Aruliah et al. (2004).

The periodograms obtained from the Lomb-Scargle analysis on the 630.0 nm line intensities from the 25 November 2003 are shown in Fig. 4. The coloured lines are the spectral power as a function of period for each of the look directions, with the same colour coding used for all plots. The horizontal lines show the 70%, 90% and 99% confidence levels. Two clear peaks with greater than 99% confidence can be seen at 1.8 and 3.7 h in all look directions in KEOPS data, most of Sodankylä and some of Skibotn. Peaks are also seen at 1.2, 1.4 and 2.5 h to varying degrees in each look direction at each site. Periods greater than about 7 h are not real, as this is greater than half the total length of the data set and so are not sufficiently sampled. Periods less than about 20 min are also not real, due to aliasing. As the same periods are seen in more than one site, this gives confidence that the periods are atmospheric effects and not instrumental. The periods are not seen so well in Skibotn data due to the low time resolution and the poor signal to noise ratio of the data. The power of the zenith data periodograms is higher than the other directions as zenith measurements were taken twice in each cycle, so the time resolution was twice as high.

The 3.7-h wave is present in all look directions in KEOPS but in Sodankylä appears in all but the south and bistatic B positions. The intensities were lower at the south and bistatic positions as these are further from the auroral oval. The detector on the KEOPS FPI is more sensitive than the Sodankylä detector which means it is able to measure lower intensities, which have a lower signal to noise ratio, more accurately. This explains the wave not being observed in the Sodankylä south and bistatic B positions while it is in KEOPS data. Skibotn sees the wave mainly in the north and south. This is consistent with the source being the auroral oval which lies across Skibotn and the north part of KEOPS and Sodankylä, as can be seen in Fig. 5 which shows the All Sky Camera (ASC) keogram for Kevo, which is near to the tristatic A point, (positions of the sites are shown in Fig. 1). Keograms take a north-south slice from the centre of each ASC image through the night and hence provide an overview of auroral activity (through a green line filter). The auroral arcs at 16:00 UT, 19:00 UT, and 23:00 UT move south and are overhead at Kevo, and so are over the KEOPS and Sodankylä north latitude. For the rest of the night the oval is to the north of Kevo. Sodankylä is south of Kevo, at about the latitude of the lower 300 km mark on this plot. As there is little activity at the bottom of the plot, overhead of Sodankylä, this means that the south and B positions are far

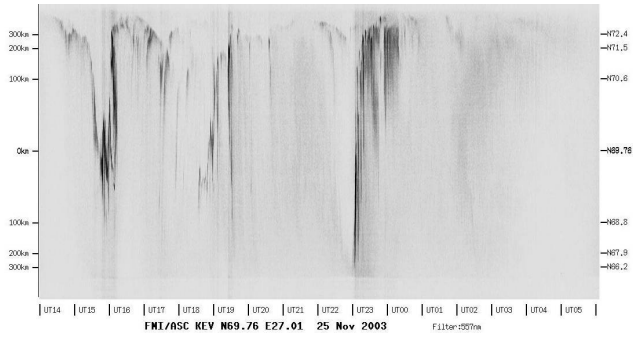

Fig. 5. All Sky Camera Keogram from Kevo for the 25 November 2003. The image shows 557.7 nm aurora, and has been made negative for clarity.

from the auroral oval. A wave of auroral source that has dissipated over the distance from the oval to the south and B positions can explain why the 3.7-h wave is not detected here. This can be explained which has an auroral source. The ASC keogram shows the oval to be on average 200–300 km north of Kevo, which would be 500–600 km north of the bistatic B and KEOPS South positions. Although gravity waves can have wavelengths of over a 1000 km (e.g. Fagundes et al., 1995, Innis et al., 2001, the source on the 25 November 2003 could be at a more distant longitude. In addition, Innis and Conde (2001) show that waves propagating poleward penetrate further than those propagating equatorward, where there are greater chances of dissipation due to background winds.

The 1.8-h wave is detected in Sodankylä south and B, but is only seen in the south in Skibotn. This implies that it either originated further south and dissipated before it could reach the more northern look directions of Skibotn; or it was propagating along the oval, in a eastward or westward direction. The former is not likely as the auroral oval was to the north, implying the wave had propagated along the auroral oval.

Figure 6 shows the amplitudes for the same data of the 25 November 2003, the neutral intensities, calculated from Eq (1). The amplitude is dependant on the power, but is also normalised with the standard deviation of the data, so it shows the size of the wave in proportion to the data. These are plotted against frequency rather than period. For both the 1.8-h (3.5 cycles/hour) and 3.7-h (1.7 cycles/hour) waves, KEOPS shows larger amplitudes to the north, which decrease towards the south, through A, east and west, zenith and the smallest amplitudes are seen at the south and B positions. This again is consistent with an auroral oval source region, which is in the north throughout the night. The relative size of the amplitudes between each of the look directions at Sodankylä are similar to those at KEOPS, which is at similar latitude, and it also has greater amplitudes to the north and A positions than the other look directions. The FPI intensities are not calibrated at present, so the intensity is dependant on detector sensitivity, so the intensities, and hence the amplitudes, are an order of magnitude smaller at Sodankylä than KEOPS. The amplitude of the 3.7-h wave is 12% of the maximum intensity at KEOPS and 11% for Sodankylä, so the wave amplitudes are comparable at both locations, as would be expected for sites at similar latitudes. The amplitudes of the 3.7-h wave in the south and B positions are very small, in agreement with the low power in the periodogram. The 3.7-h wave in Skibotn data has similar amplitudes in all look directions. The north direction again has the largest amplitude, but this is consistent with the keogram from Ny Ålesund on Svalbard in the polar cap (not shown), which shows activity, confirming that the oval spreads across this whole region observed. The auroral oval covers all of the look directions for Skibotn. The 2.5-h wave is more prominent than the 1.8-h wave. The keogram for Ny Ålesund (not shown) in Svalbard shows activity slightly to the south of the site, showing that the auroral oval covers latitudes in the whole of the area covered by the Skibotn FPI, which is consistent with all look directions showing the wave with large amplitudes.

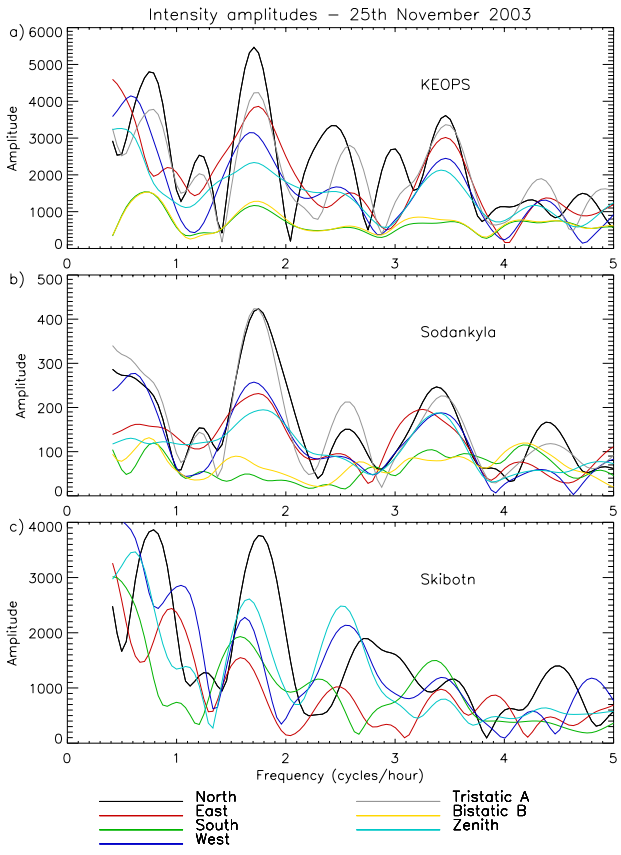

Fig. 6. Amplitudes of Lomb-Scargle periodograms for FPI intensities for **(a)** KEOPS, **(b)** Sodankylä, and **(c)** Skibotn, on the 25 November 2003.

To view the periodicities in the wind data from the FPIs, the data first need to be smoothed. This is because the two-cell pattern of thermospheric winds due to magnetospheric

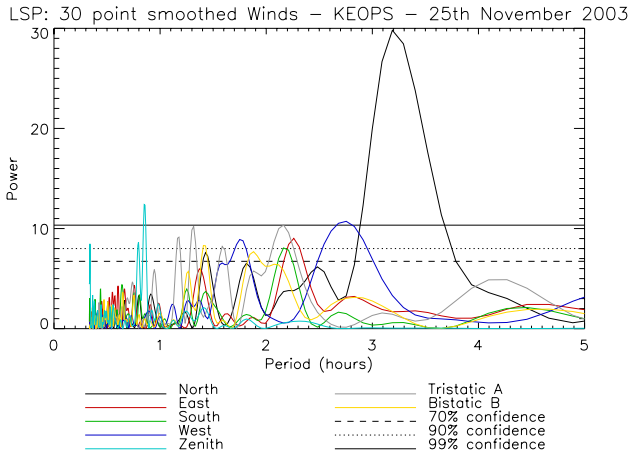

Fig. 7. Periodogram from KEOPS wind data with a 30 point (∼10 min) smoothed value removed, for the 25 November 2003.

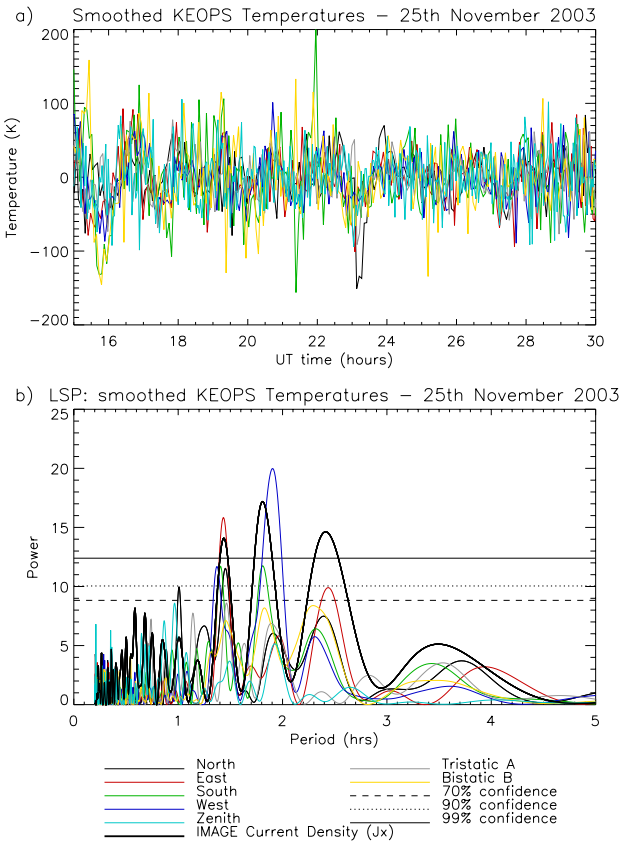

Fig. 8. Neutral temperatures with a 2 h smoothed value removed **(a)** and their periodogram **(b)** from KEOPS from the 25 November 2003. The bottom plot also shows the periodogram for the equivalent current densities (thick black line) from IMAGE data (smoothed and reduced by a factor of 2 for comparisons).

convection across the polar cap creates a predominantly westward wind in the evening sector and eastward in the morning hours. This means that the majority of the power of the periodogram goes into this 12- h period wave-like pattern. To compensate for this, a 30 point running smoothing of the data is subtracted from the data. This corresponds to an approximately 120 min smoothing. This value is used as it removes the low frequency variations, and so removes power from the longest periods, i.e. those likely to be associated with atmospheric tides, but is also not so small as to remove power from the periods of interest. These data, normalised for diurnal variations, for KEOPS on the 25 November 2003 are shown in Fig. 7. This shows a strong wave with a period of 3.1 h in the north winds, but does not show the 1.8 and 3.7-h waves seen in the intensities. Many other periods above the 70% confidence level are seen though, at 0.8, 1.1, 1.3, 1.4, 1.6, 1.7, 2.2, 2.3 and 2.8 h. Although only two of these (the 1.4 and 2.1 h waves) are observed with confidence levels greater than 70% in two look directions, several are observed in several look directions but with lower spectral powers. The 1.3 and 1.4 h waves are also seen in Sodankylä data (not shown) at 70% confidence levels with a 40 min smoothing, as are the 2.2 and 2.3 h waves with 80 min smoothing at 90% confidence, and 2.8 and 3.1 h with 120 min smoothing. Gravity waves in the winds are complicated by the fact that the wave equations are dependant on the background winds (Nappo, 2002; Lindzen, 1990). The frequencies of waves that are present in the intensities are therefore not necessarily expected to be present in the wind speeds. Innis and Conde (2001) observed gravity waves in vertical winds from the DE2 satellite. However, the FPI data presented here is believed to be the first observation of gravity waves detected in the horizontal upper thermospheric winds.

Smoothing the data is also useful for identifying waves in the thermospheric temperatures. Gradients are often seen over a night, as the temperatures are relatively slow to respond to changes in geomagnetic activity levels. Figure 8 shows the results for the temperatures from the same night of the tristatic campaign, from KEOPS. Figure 8a is the data smoothed with a 30 point running average, subtracted from the absolute temperatures. A wave structure can be clearly seen in the temperatures, and in all the look directions. The waves end at 04:00 UT, which is just due to the sky becoming overcast at this time. The periodogram is shown in Fig. 8b. The periodicities in the different look directions are not quite as well defined as for the intensities and winds, but are within the minimum error, of 4.5 min between data points. The most predominant periods are at 1.4, 1.8 and 2.3 h, with other periods above the 70% confidence level at 1.0, 1.1 and 1.3 h. These periods are also seen in the data before being smoothed, though with lower powers as long period waves have high spectral powers. Also on this plot is the periodogram of the equivalent current densities, calculated from the IMAGE magnetometer network. This is discussed further in Sect. 3.2 below. The response time of

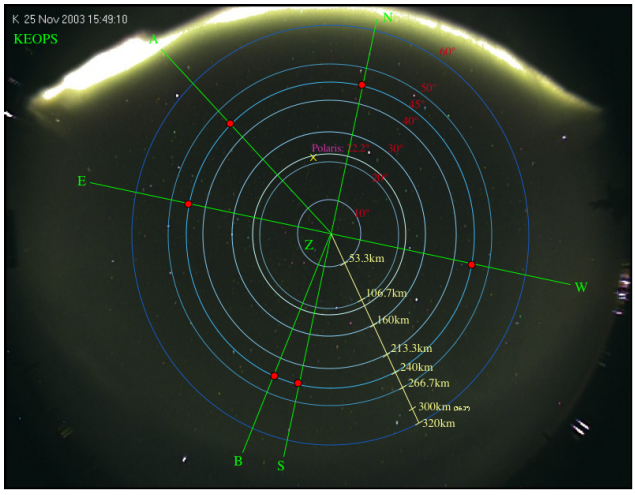

Fig. 9. All-Sky Camera image from KEOPS on the 25 November 2003, showing an auroral arc to the north of KEOPS. Green lines show the look directions; red dots show the 630.0 nm emitting volume presuming a 240 km height; circles show other height distances.

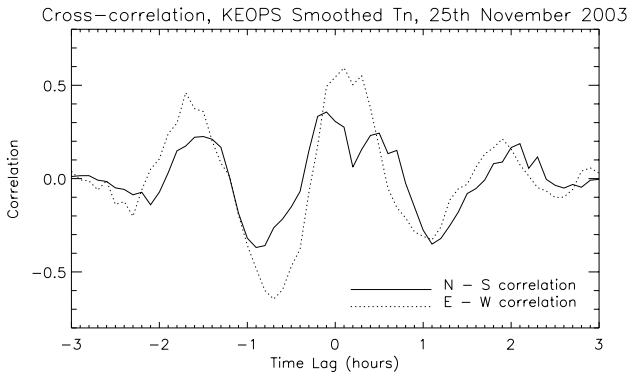

Fig. 10. Cross correlations between north and south (solid line) and east and west (dotted line) smoothed neutral temperatures from KEOPS on the 25 November 2003.

the three parameters are different, but it is not clear whether the same periodicities would be expected in the winds as intensities, and this will be investigated further by a statistical survey of the FPI data sets.

Williams et al. (1993) studied data taken as part of the World-Wide Atmospheric Gravity Wave Study (WAGS) campaign. They show that two bursts of particle precipitation could cause gravity waves of the same period as the time between the precipitation periods. The two times of strongest particle precipitation on the night of the 25 November 2003 in Fig. 3 were at 19:27 and 23:15 UT. These times are 3.7 h apart, and correspond to one of the strongest periods seen in the periodogram for that data. The smoothed temperatures in Fig. 8a show that the waves start before the start of the data set, i.e. before the first period of precipitation seen in the intensities at 19:27 UT. However, APL has a colour All-Sky Camera (ASC) at the site of the KEOPS FPI. Data is available for this night from as soon as the Sun sets. The FPIs require lower background light levels and so data is only collected from an hour after sunset. An image from the ASC 3.7 h before the first period of precipitation seen in the FPI intensities is shown in Fig. 9, at 15:49 UT on the 25 November 2003. This figure also shows the positions of the FPI viewing volumes. Green lines show the look directions (north (N), east (E), south (S), west (W), zenith (Z), and tristatic (A) and bistatic (B) positions with Sodankylä. The red dots show the 630.0 nm emitting volume observed presuming a 240 km emission height and circles show the distance of this region assuming different emission altitudes. This image shows an auroral arc to the north of KEOPS, which again agrees with the amplitudes of the waves (Fig. 6) being larger to the north. This image showing auroral precipitation is 6.63 h before the first period of precipitation seen in the FPI data (at 19:27 UT). The ASC images show a third period of precipitation this night, at 23:09 UT – 3.70 h after the second. The ASC data images are taken every 5 min, so these periods are the same as the FPI periodograms within errors, which are a minimum of 0.08 h for KEOPS data. This therefore corroborates the theory of Williams et al., (1993) that the 3.7-h wave is created from forcing from evenly spaced bursts of heating due to particle precipitation.

There are no periods of enhanced precipitation in the intensities (Fig. 3) at 1.2, 1.8 or 2.5 h apart, to produce these other peaks. Therefore, heating from precipitation does not seem to be a likely cause of the gravity waves on this night, other than for the 3.7-h period wave. Evidence for the alternative mechanism via electrojet activity is described in Sect. 3.2 below.

A cross correlation was performed on the smoothed neutral temperatures to obtain the phase speed and direction and horizontal wavelength (see Eq. 2). The peaks of the curves obtained give the zonal and meridional lags, τ_x and τ_y respectively (Oliver et al., 1994). To perform the cross correlation, the data from the two look directions need to be at the same times, therefore the data were interpolated, to 0.1-h intervals. The first two hours of observations of the temperatures, when smoothed (Fig. 8a), show just the 1.8-h period wave, so this period (14:24–17:30 UT) is used to determine the wave parameters. The results of this are shown in Fig. 10. This shows a lag for the east – west correlation (dotted line), but the north – south correlation (solid line) shows a dip in the peak so that the lag cannot be determined. Figure 11 shows the temperatures after they have been smoothed again with a 40-min running smoothing, to decrease the noise levels further so that the peaks can be better determined. By examination of these smoothed temperatures, it can be seen that the north direction shows a skew between 15:00 UT and 16:00 UT, and it has been determined by removal of this skew that this is the cause of the dip in Fig. 10. This is likely to be

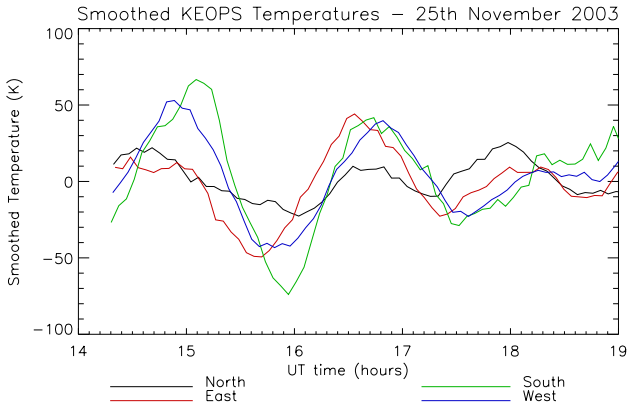

Fig. 11. Neutral temperatures with a 2 h smoothed value removed, then with a secondary 40 min smoothing, from KEOPS on the 25 November 2003.

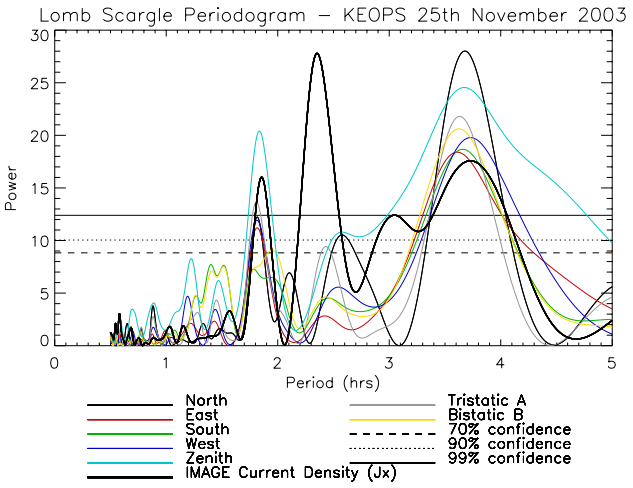

Fig. 12. The LSP for FPI intensities from KEOPS from the 25 November 2003. The periodogram for the equivalent current densities from IMAGE data (thick black line) has a 200 min smoothing removed, and the periodogram was divided by 4 for comparisons.

due to the superposition of another wave on top of the 1.8-h wave that can be clearly seen. This will also be the cause of the shift of the peak at 16:30 UT as the beginning part of the peak is removed as it is decreased by the secondary wave. This will also account for the smaller amplitude of this wave at this time.

Therefore, to determine the lags, the peaks between 14:00 UT and 15:00 UT are used. This gives values of 0.5 h for τ_x and 0.2 for τ_y. Using Eq. (2), and a distance between the look directions of 480 km, gives a phase speed of $250\pm50\,\mathrm{ms}^{-1}$ and a phase angle θ of $302°\pm15°$ measured as the direction the wave is travelling, at an angle clockwise from the north. It is therefore propagating in a south-south-westward direction, consistent with an auroral oval source as this is to the north at this time. For the wave with period 1.8 h, this gives a horizontal wavelength, λ_h of 1600 km. This is consistent with previous observations and theory of TIDs, for example Hocke and Schlegel (1996).

The fact that there is a lag between the different look directions is also evidence that the oscillations are due to gravity waves, rather than being, for instance, an atmospheric tide that has been modulated by a planetary wave. Tides and planetary waves are large-scale phenomena with very large horizontal wavelengths of several thousand kilometres. These would therefore not vary over the scale of the distance between look directions, which for one site is around 480 km.

3.2 Electrojets

To investigate whether Joule heating from the electrojets could be the generation mechanism of the other period gravity waves, IMAGE magnetometer data were analysed. Electrojet activity does not necessarily coincide with the location of particle precipitation, so this would give a different source and provide different periodicities to a precipitation source. There are many magnetometer stations across Scandinavia, including at the sites of the FPIs and EISCAT radars. Periodograms on the ground magnetic field perturbations B_x, B_y and B_z components) do not produce periods with much correlation to the FPI data. However, due to the large array of magnetometer stations, equivalent current densities can be calculated (Pulkkinen et al., 2003). This gives values, for J_x (north component) and J_y (east component), in A/km. Values are calculated along a line of longitude through the centre of the magnetometer stations, and at an altitude of 100 km. LSPs are therefore performed on data near the position of Kiruna (at 68.62° N, 22.06° E).

The thick black line in Fig. 8b is the periodogram for the J_x component of the equivalent current densities. Data from 14:00–24:00 UT on the 25 November 2003 were used. 80 min smoothed data was subtracted from the data before the periodogram was calculated, to again increase powers in the shorter periods. This was done with the same method as for the FPI data. The LSP for the equivalent current densities, divided by a factor of 2, is plotted over the periodograms for the normalised temperatures, for comparisons. A very good match can be clearly seen with many of the periodicities detected. The strong periods at 1.4, 1.8, and 2.4 h are seen in the LSPs of the equivalent current densities as well as the temperatures. Even some of the shorter periods are seen, such as those at 0.8, 1.0 and 3.5 h. The 3.5-h peak has a lower power for the temperatures than the 630.0 nm intensities due to the smoothing, which takes power out of the longer periods but allows the shorter periods to be seen more clearly.

Figure 12 shows the periodogram for the KEOPS FPI intensities, with the smoothed current density overlaid with a thick line as for the temperatures. J_x component from 12:00 UT–06:00 UT is used, with a 200 min smoothed value removed, and scaled down by a factor of four, for comparisons. The LSP for the equivalent current densities has a

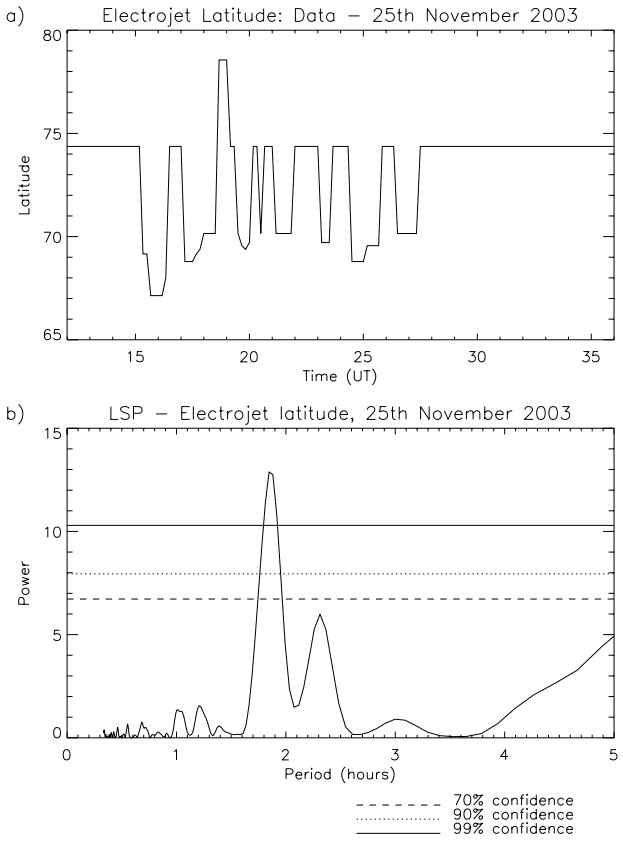

Fig. 13. Positions of the electrojets **(a)** and periodogram **(b)** from IMAGE B_z data, from the 25 November 2003.

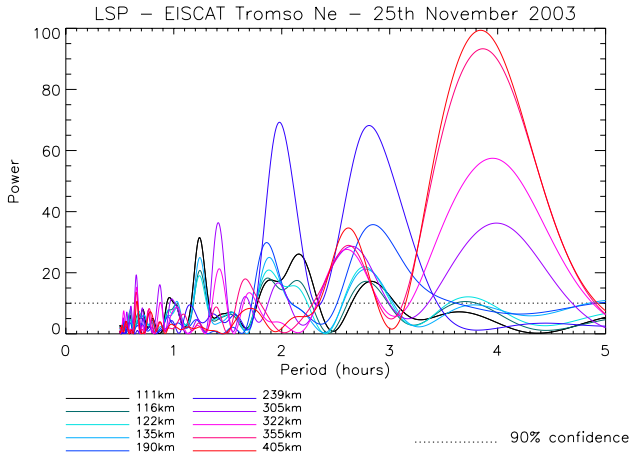

Fig. 14. Lomb-Scargle Periodogram from EISCAT electron densities from the 25 November 2003. Colours are for different heights along the Tromsø beam.

larger power because it has approximately four times higher time resolution, with data points every minute. The 1.8 and 3.7 h peaks match very well, but there is also a large peak at 2.4 h that is not seen in the intensities. The 3.7 h wave has a higher power here than in Fig. 8b, as the intensities are not smoothed, since there are no long term trends as are seen in the winds and temperature data over a night.

By comparing the vertical perturbations B_z from magnetometers at different latitudes, the position of the centre of the electrojet can be determined as a function of local time, i.e. its variation in latitude. At the location of the westward electrojet, the B_z component to the north will be decreased, and increased to the south. Conversely, for the eastward electrojet, B_z will increase to the north and decrease to the south. Figure 13a shows the latitudinal location of the centre of the electrojet through the night, estimated at 10-min intervals. A Lomb-Scargle analysis for these, gives the periodogram in Fig. 13b. This shows periods of 1.8 and 2.3 h, which correspond to the smoothed temperature periods from KEOPS.

3.3 Ion-neutral coupling

Due to the relative difficulty in obtaining thermospheric data with respect to ionospheric data, thermospheric gravity waves have often been studied using neutral data derived from ionospheric measurements, such as radar data. As these measurements are not independent, the coupling between the ions and neutrals cannot properly be studied. However, for the night of the 25 November 2003 the EISCAT UHF radars were in tristatic mode, viewing the same volume of sky as the FPIs at the tristatic point above KEOPS. This provides a good opportunity to study gravity waves and their ionospheric counterpart, TIDs, at the same time. STARE (part of the MIRACLE network) coherent scatter radar data are also available for this period.

The EISCAT UHF data from the 25 November 2003 was shown in Fig. 2 and the wavefronts that can be seen were described in Sect. 3.1. Lomb-Scargle analyses of the electron densities N_e from Tromsø data at different altitudes are shown in Fig. 14. The altitudes shown range from the E-region, in greens and blues up to high F-region altitudes, in reds. 111 km (dark green) is the nearest range gate to the equivalent current densities of the magnetometer data. The highest altitude shown is at 405 km in red.

The height of the maximum electron density in the F-region (hmF2) is shown in Fig. 15 in grey. The 630.0 nm emission is estimated as being 50 km (approximately one scale height) below hmF2 (an hourly smoothed value is plotted). The emission altitude is approximately one scale height thick, and the peak can be seen to vary between 230 km – 300 km over this night. The altitudes corresponding to this in the EISCAT LSPs (Fig. 14) are shown in blue and purple (239 km and 305 km).

The periods seen in the EISCAT data (Fig. 14) match several of those seen in the FPI data. The first periodicity

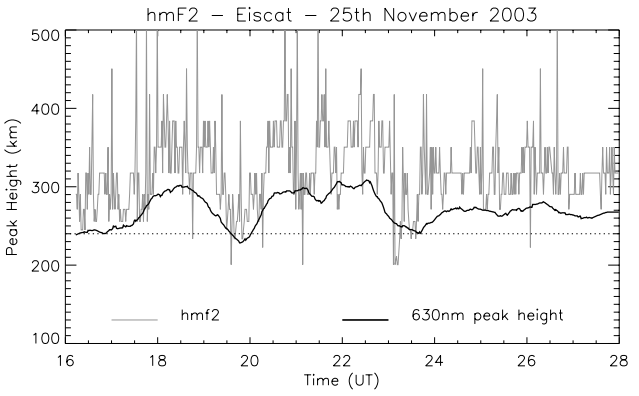

Fig. 15. EISCAT hmF2 values for the 25 November 2003 (grey) and estimated OI emission altitude (black). The presumed altitude of 240 km is shown with a horizontal dotted line.

seen in N_e data above the 90% confidence level, which is at 0.6 h, however is not present in FPI data. The period with a strong power at 1.2 h is only seen in the lower altitudes, from 111 km–135 km. This period is weakly seen in the current densities, in Fig. 8, but not strongly in the FPI data. This could imply that it has dissipated by the time it reaches the 630.0 nm emission altitude.

The 1.5-h wave that is seen in the FPI temperatures and the electrojet, from the equivalent current densities, is also seen in the upper altitudes of EISCAT N_e data. This may possibly indicate that there is a vertical component in the direction of propagation of this wave. The STARE coherent scatter radar (Greenwald et al., 1978) provides electric field values, which are also at the electrojet altitude. The LSP for the Ex values (geomagnetic north component, in mV/m) is shown in Fig. 16. This shows the periodogram powers in colour, for all the latitudes in the STARE radars field of view, at a longitude of 20.4° E, which is the location of the KEOPS FPI. The horizontal lines mark the latitudes of KEOPS (full line) and the tristatic A point and the Skibotn north location, which is the northernmost look direction of the three FPIs. Vertical yellow lines mark waves with periods of 1.5, 1.8, 2.3 and 3.3 h. This therefore shows that the 1.5 h wave is likely to be of electrojet origin as it is seen in the electrojet equivalent current densities and the electric fields, both at E-region heights.

The 1.8-h wave, seen in both the FPI intensities and temperatures, is also seen in the N_e LSP (Fig. 14) in the E and lower F region heights (up to about 290 km). This 1.8-h peak is not seen in the highest altitudes, and not above about 300 km. This period is also present in the electrojets (Fig. 13), equivalent current densities (Fig. 12), and electric fields (Fig. 16b) all of which are at E-region altitudes. This therefore agrees with an electrojet source of the wave, which has dissipated by the time it reaches higher F-region altitudes, higher than the FPI observing height.

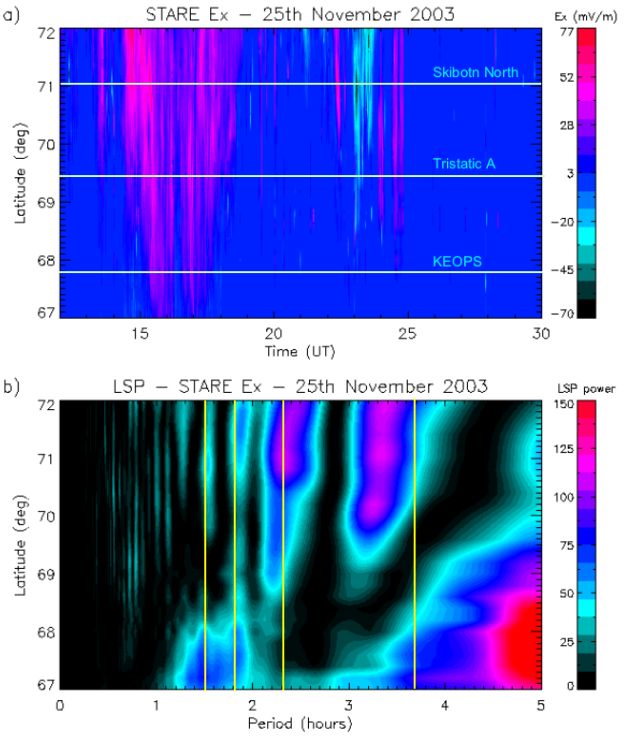

Fig. 16. STARE electric field (northwards component) for the 25 November 2003 (top) and LSP (bottom), at a longitude of 20.4° E. The latitudes of KEOPS, the tristatic A point, and the northernmost extent of the FPI data are marked with horizontal lines in the top plot. Vertical lines highlight some of the waves present in the LSP.

The fact that the 1.2 h wave seen in the N_e LSP is not observed in the FPI data, but the 1.8 h wave is, which is also of an electrojet source, could imply that they have different limits to their propagation distances. The amplitudes of the two waves (not shown) are very similar. The STARE data (Fig. 16b) shows the 1.2-h wave in the lowest and highest latitudes, but not very strongly at the FPI data latitudes (shown on Fig. 16a).

There are two overlapping periodicities in Fig. 14 from 2.5 to 3 h. The higher altitudes, from 305 km peak at 2.6 h, but below this, the peak moves to nearer 2.9 h. The equivalent current density LSP has a peak at 2.4 h, and the STARE electric fields have peaks at 2.3 h at high latitudes, from the tristatic A point and further north (Fig. 16), and the position of the electrojets (Fig. 13b) shows a periodicity of 2.3 h. Both the FPI intensities and temperatures have periodicities that differ in the different look directions, ranging from 2.3 to 2.6 h. The tristatic A point temperatures has a small peak at 2.8 h, but this is below the 70% confidence level. Whether these are superimposed waves or one wave with a varying source is unclear.

The 3.7-h wave only occurs at the higher altitudes in the EISCAT N_e data (Fig. 14), from 300–500 km. As the 3.7-h wave is not seen in the lower altitudes, this shows that

it is unlikely to be a wave of electrojet source, as this is at lower heights and the wave would be expected to be stronger here. This periodicity is not seen in the magnetometer or STARE electric field data at E-region heights. The magnetometer data will show the height integrated currents, and so will be dominated by the E-region. This therefore implies an auroral precipitation source region, at high altitudes, and therefore from lower energy particles. This agrees with ASC data shown in Sect. 3.1.

4 Conclusions

Gravity waves are detected in the high latitude thermosphere in neutral winds and temperatures as well as in atomic oxygen emission intensities. Previous work on observations of thermospheric gravity waves (e.g. de Deuge et al., 1994; Innis et al., 2001) used photometer data, so only had 630.0 nm intensities. Innis and Conde (2001) observed gravity waves in vertical thermospheric winds from satellite (DE2) data. This is therefore believed to be the first detection of gravity waves in upper thermospheric temperatures. Their work was also in the Southern polar cap region, whereas these data are from northern latitudes and from the auroral oval region. The Scandinavian region also has the advantage of being covered by a range of other instrumentation.

Gravity waves of a variety of periods have been detected using a Lomb-Scargle analysis, with periods of order of a few hours. The gravity waves were seen in thermospheric intensities, winds and temperatures from Fabry-Perot interferometer measurements of the 630.0 nm atomic oxygen line. The amplitudes of the waves show that the data are consistent with an auroral source region.

Two mechanisms have been proposed (de Deuge et al., 1994) for the formation of thermospheric gravity waves – Joule heating from particle precipitation and heating from electrojet currents. For the data presented here, from the 25 November 2003 from the Scandinavian sector, waves of several periods have been found. There is evidence that these waves have different source mechanisms. It has been shown that for this data set that heating from particle precipitation is the likely source mechanism for a wave of period 3.7 h. Two periods of precipitation are seen in the FPI intensities, also separated by 3.7 h. Although the first of these periods of precipitation occur after waves are seen in the temperatures, an auroral arc is seen in all sky camera images 3.7 h before this. This therefore suggests that these periods of precipitation are driving the wave, as proposed by Williams et al. (1993). The amplitudes of the waves are greater to the north of the region, which is where the auroral activity is observed. This too supports an auroral source region.

For the other periodicities seen in these data, of 1.2, 1.5, 1.8 and 2.5 h, it is proposed that the source of the gravity waves is Joule heating from electrojet activity. The Lomb-Scargle analysis performed on equivalent current densities, as well as the position of the electrojet, calculated from magnetometer data from the IMAGE chain, reveal periodicities similar to those found in the FPI data. Periodicities seen in the FPI temperature data are very well matched by the periods found from the J_x component of the equivalent current densities, showing that the strength of the electrojet is the cause of the gravity waves observed. Cross correlations of the neutral temperatures were used to find that the phase speed of the 1.8 h wave to be 250 ms^{-1} with a phase angle θ of 302°, which gives a horizontal wavelength, λ_h of 1600 km. This is both consistent with previous TID measurements and with an auroral oval source region.

The gravity waves found in the FPI thermospheric data have also been compared with the TIDs found in radar data. EISCAT incoherent scatter data provides electron densities and ionospheric wind speeds and temperatures. STARE coherent scatter radars provide electric field data, which can be used to identify gravity waves at E-region altitudes. These data sets confirm the source of the waves with periodicities of 1.2, 1.5 and 1.8 h to be from Joule heating from electrojet currents, and the 3.7-h wave to be of higher altitude in origin, and therefore from particle precipitation localised heating. These complementary data sets therefore show that on the 25 November 2003 waves of several different periodicities were present, and that different source mechanisms produced the different waves.

Data presented here are of a case study of the night of the 25 November 2003. Gravity waves have also been seen in FPI data from several other nights, and from the Svalbard FPI in the polar cap as well as the mainland Scandinavia FPIs in the auroral oval regions. Future work will be to make a statistical study of the gravity waves found in all the sets of FPI data. Data are available for the winter months from both locations for the last 7 years, and from Kiruna since 1981, so this will provide a large possible number of clear nights to study.

Acknowledgements. The FPIs were built and maintained with thanks to PPARC, grant PPA/G/O/2001/00484. We also wish to acknowledge the ESRANGE KEOPS facility, the Sodankylä Geophysical Observatory and LAPBIAT grant for their generous help in logistics. EISCAT is an International Association supported by Finland (SA), France (CNRS), Germany (MPG), Japan (NIPR), Norway (NFR), Sweden (VR), and the United Kingdom (PPARC). Thanks to the Rutherford Appleton Laboratory for EISCAT data analysis. The MIRACLE network is operated as an international collaboration under the leadership of the Finnish Meteorological Institute. The IMAGE magnetometer data are collected as a Finnish-German-Norwegian-Polish-Russian-Swedish project, with thanks to A. Viljanen (FMI) for the equivalent current densities.

Topical Editor M. Pinnock thanks two referees for their help in evaluating this paper.

References

Arnold, N. F., Jones, T. B., Robinson, T. R., Stocker, A. J., and Davies, J. A.: Validation of the CUTLASS HF radar gravity wave observing capability using EISCAT CP-1 data, Ann. Geophys., 16, 1392–1399, 1998.

Aruliah, A. L., Griffin, E. M., Aylward, A. D., Ford, E. A. K., Kosch, M. J., Davis, C. J., Howells, V. S. C., Pryce, E., Middleton, H., and Jussila, J.: First direct evidence of meso-scale variability on ion-neutral dynamics co-located tristatic FPIs and EISCAT radar in Northern Scandinavia, Ann. Geophys., 23, 147–162, 2005.

Aruliah, A. L., Griffin, E. M., McWhirter, I., Aylward, A. D., Ford, E. A. K., Charalambous, A., Kosch, M. J., Davis, C. J., and Howells, V. S. C.: First tristatic studies of meso-scale ion-neutral dynamics and energetics in the high-latitude upper atmosphere using collocated FPIs and EISCAT radar, Geophys. Res. Lett., 31, L03802, doi:10.1029/2003GL018469, 2004.

Aruliah, A. L. and Griffin, E. M.: Evidence of meso-scale structure in the high latitude thermosphere, Ann. Geophys. 19, 37–46, 2001.

Balthazor, R. L. and Moffett, R. J.: Morphology of large-scale travelling atmospheric disturbances in the polar thermosphere, J. Geophys. Res., 104, 15–24, 1999.

de Deuge, M. A., Greet, P. A., and Jacka, F.: Optical observations of gravity waves in the auroral zone, J.Atmos. Terres. Phys., 56, 617–629, 1994.

Fagundes, P. R., Aruliah, A. H., Rees, D., and Bittencourt, J. A.: Gravity wave generation and propagation during geomagnetic storms over Kiruna (67.8° N, 20.4° E), Ann. Geophys., 13, 358–366, 1995.

Greenwald, R. A., Weiss, W., Neilsen, E., and Thomson, N. R.: STARE: A new radar auroral backscatter experiment in northern Scandinavia, Radio Sci., 13, 1021–1039, 1978.

Hargreaves, J. K.: The Upper Atmosphere and Solar – Terrestrial Relations, Berkshire, Van Nostrand Reinhold Co. Ltd., 1979.

Horne, J. H. and Baliunas, S. L.: A prescription for period analysis of unevenly sampled time series, Astrophys. J., 302, 757–763, 1986.

Hocke, K. and Schlegel, K.: A review of atmospheric gravity waves and travelling ionospheric disturbances: 1982–1995, Ann. Geophys., 14, 917–940, 1996.

Hocke, K.: Phase estimation with the Lomb-Scargle periodogram method, Ann. Geophys., 16, 356–358, 1998.

Hunsucker, R. D.: Atmospheric gravity waves generated in the high-latitude ionosphere: a review, Rev. Geophys. Space Phys., 20, 293–315, 1982.

Innis, J. L. and Conde, M.: High-latitude thermospheric vertical wind activity from Dynamics Explorer 2 Wind and Temperature Spectrometer observations: Indications of a source region for polar cap gravity waves, J. Geophys. Res., 107, 1172, doi:10.1029/2001JA009130, 2002.

Innis, J. L. and Conde, M.: Thermospheric vertical wind activity maps derived from Dynamics Explorer-2 WATS observations, Geophys. Res. Lett., 28, 3847, 2001.

Innis, J. L., Greet, P. A., and Dyson, P. L.: Thermospheric gravity waves in the southern polar cap from 5 years of photometric observations at Davis, Antarctica, J. Geophys. Res., 106, 15 489, 2001.

Lanchester, B. S., Nygen, T., Jarvis M. J., and Edwards R.: Gravity wave parameters measured with EISCAT and Dynasonde, Ann. Geophys., 11, 925–936, 1993.

Lindzen, R. S.: Dynamics in Atmospheric Physics, Cambridge, Cambridge University Press, 1990.

Lomb, N. R.: Least squares frequency analysis of unequally spaced data, Astrophys. Space Sci., 39, 447, 1976.

MacDougall, J. W., Andre, D. A., Sofko, G. J., Huang, C. S., and Koustov, A. V.: Travelling ionospheric disturbance properties deduced from Super Dual Auroral Radar measurements, Ann. Geophys., 18, 1550, 2001.

Mitchell, N. J. and Howells, V. S. C.: Vertical velocities associated with gravity waves measured in the mesosphere and lower thermosphere with the EISCAT VHF radar, Ann. Geophys. 16, 1367, 1998.

Nappo, C. J.: An Introduction to Atmospheric Gravity Waves, California, Academic Press, 2002.

Oliver, W. L., Fukao, S., Yamamoto, Y., Takami, T., Yamanaka, M. D., Yamamoto, M., Nakamura, T., and Tsuda, T.: Middle and upper atmosphere radar observations of ionospheric density gradients produced by gravity wave packets, J. Geophys. Res., 99, 6321–6329, 1994.

Oliver, W. L., Fukao, S., Sato, M., Otsuka, Y., Takami, T., and Tsuda, T.: Middle and upper atmosphere radar observations of the dispersion relation for ionospheric gravity waves, J. Geophys. Res., 100, 23 763–23 768, 1995.

Press, W. H. and Rybicki, G. B.: Fast algorithm for spectral analysis of unevenly sampled data, Astrophys. J., 338, 277–280, 1989.

Pulkkinen, A., Amm, O., and Viljanen, A.: and the BEAR working group, Ionospheric equivalent current distributions determined with the method of spherical elementary current systems, J. Geophys. Res., 108, 1053, doi:10.1029/2001JA005085, 2003.

Rishbeth, H. and Williams, P. J. S.: The EISCAT Ionospheric Radar: the System and its Early Results, Quart. J. Royal Astronom. Soc., 26, 478–512, 1985.

Scargle, J. D.: Studies in Astronomical time series analysis: II Statistical aspects of spectral analysis of unevenly spaced data, Astrophys. J., 263, 835–853, 1982.

Shibata, T. and Schlegel, K.: Vertical structure of AGW associated ionospheric fluctuations in the E- and lower F-region observed with EISCAT – A case study, J. Atmos. Terr. Phys., 55, 739–749, 1993.

Solomon, S. C., Hays, P. B., and Abreu, V. J.: The auroral 6300A emission: observations and modeling, J. Geophys. Res., 93, 9867, 1988.

Viljanen, A. and Häkkinen, L.: IMAGE magnetometer network, in: Satellite-Ground Based Coordination Sourcebook, edited by: Lockwood, M., Wild, M. N., and Opgenoorth, H. J., ESA publications SP-1198, 111–117, 1997.

Williams, P. J. S., Virdi, T. S., Lewis, R. V., Lester, M., Rodger, A. S., McCrea, I. W., and Freeman, K. S. C.: Worldwide atmospheric gravity-wave study in the European sector 1985–1990, J. Atmos. Terr. Phys., 55, 683–696, 1993.